Highlights

Data-driven rheological model for 3D printable concrete

Jianhao Gao,Chaofeng Wang,Jiaqi Li,S.H. Chu

- Analyzed the rheology of 3D printing concrete through the lens of data.
- Identified research gaps in the area of mix designs for 3D printing concrete.
- Developed novel predictive models for 3D printing concrete and explained the models using game theory.
- Developed novel explicit equations for rapid estimation of rheological properties based only on the mix design.

Data-driven rheological model for 3D printable concrete

Jianhao Gao[a], Chaofeng Wang[a,b,*], Jiaqi Li[c] and S.H. Chu[d]

[a] *M.E. Rinker, Sr. School of Construction Management, College of Design, Construction and Planning, University of Florida, FL, USA*

[b] *Department of Civil & Coastal Engineering, Herbert Wertheim College of Engineering, University of Florida, FL, USA*

[c] *Atmospheric, Earth, & Energy Division, Lawrence Livermore National Laboratory, Livermore, CA, USA*

[d] *Department of Civil Engineering & Engineering Mechanics, Columbia University, New York, NY, USA*

ARTICLE INFO

Keywords:
3D printing concrete
rheology
data-driven
data mining
mix design

ABSTRACT

Additive manufacturing in construction demands an in-depth understanding of the rheological properties of fresh concrete. However, the abundant data in this field remains underexplored. This conventional fragmented approach has hindered broader progress and innovation. This study aims to develop rheological models for 3D printable concrete through a comprehensive, data-driven paradigm, emphasizing the urgent need for a unified, large-scale dataset. By compiling data spanning a decade, we have created an open-access dataset that contains mix designs and experimental results on the rheological behaviors of additive construction concrete. A machine learning-based model and explicit polynomial expressions for estimating rheological properties were developed. The developed machine learning model can take nineteen different parameters as inputs to predict the rheological behavior of printed concrete, showing superiority over models considering a few parameters. Our model can predict the properties of unexplored mix designs, with tailored expressions for practical engineering in additive construction. This enhances understanding of concrete mix design and rheology, highlighting the importance of data-driven method in unveiling the complexity of concrete.

1. Introduction

Additive construction, or three-dimensional (3D) concrete printing, i.e., 3DCP, is considered a technique possessing great potential for automation in construction [1, 2]. The main process is the pumping and extrusion of fresh concrete to form a structure layer by layer. The process requires the fresh concrete to be easily pumpable, extrudable, and buildable - attributes intimately linked to its rheological properties [3–5]. However, such requirements often lead to conflicting rheological demands. For example, the pumpability requires low plastic viscosity to ensure the easy flow during the transportation under a specific working pumping pressure, while the buildability requires high viscosity so that the printed fresh concrete can maintain its shape without the external support from the framework - a main advantage of 3DCP compared with traditional construction. The pumpability and extrudability both demand a relatively low dynamic yield stress to allow the concrete to flow, while the buildability demands high static yield stress so that the

*Corresponding author: chaofeng.wang@ufl.edu

concrete can maintain a stable shape once printed. To meet these requirements, accurately designing rheological properties is critical in achieving the desired balance.

The importance of rheology optimization has been sufficiently addressed in previous research [6–9]. The inherent relationships between ingredients and rheology are pivotal in guiding the mix design process [10–13]. Traditionally, this process involves a trial-and-error approach, featured with extensive lab tests to fit the Bingham plastic model [14]. This model can be mathematically expressed as:

$$\tau = \tau_y + \mu\dot{\gamma} \tag{1}$$

where τ is the shear stress in units of kPa, τ_y is the dynamic yield stress in units of kPa, μ is the plastic viscosity in units of $\mathrm{Pa \cdot s}$, and $\dot{\gamma}$ is the shear rate in units of s^{-1}.

The dynamic yield stress represents the critical shear stress level below which the shear stress is inadequate to sustain the flow, the plastic viscosity indicates the increase of stress with flow speed. Along with the two parameters, static yield stress, the minimum shear stress to initiate the flow, is also an important property. Figure 1 shows a typical experiment [5, 13, 15] for measuring them, where Bingham model is applied to find the dynamic yield stress and plastic viscosity, while the static yield stress is obtained from the peak stress during the loading process.

However, traditional experiment-based trial-and-error approach to mix design could be time consuming and labor-intensive. Alternatively, behavior of concrete can be predicted directly based on its mix design - these are pure data-driven methods, where data is used to fit a statistical relationship between the mix design and the hardening or rheological properties. For hardening properties, Yeh [16] pioneered this research using neural networks to predict concrete compressive strength in 1998. In recent years, Song et al. [17] employed a neural network model to predict the strength of concrete and used the model for selecting lower-carbon mix designs. Emad et al. [18] used Linear regression, pure quadratic, M5P-tree, and neural network to predict the compressive strength of Ultra-High-Performance Fibre Reinforced Concrete and compared with experimental results. Ahmed et al. [19] employed several machine learning techniques, including artificial neural networks, multi-expression programming, full quadratic regression, linear regression, and M5P-tree, to predict the compressive strength of geopolymer concrete. Naseri et al. [20] introduced

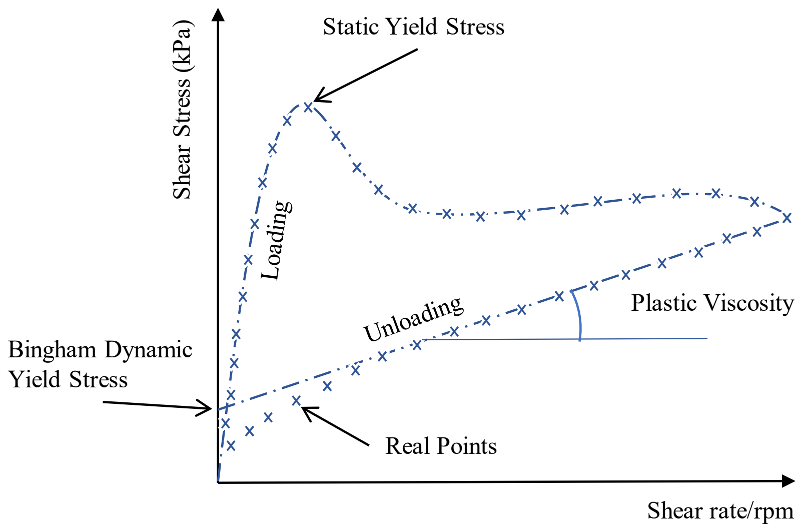

Figure 1: Typical static yield stress, dynamic yield stress and plastic viscosity experimental measurement

Coyote Optimization Programming to predict the compressive strength of concrete incorporating supplementary cementitious materials (SCMs). They also modeled an optimization problem to evaluate the compressive strength, cost, and environmental impact of sustainable concrete mixtures. Huang et al. [21] developed gradient-boosted regressors to predict concrete properties for the optimization of strength, cost, and CO_2 emissions. Kakasor Ismael Jaf et al. [22] analyzed data from various sources and used four models to predict compressive strength. They found that increasing SiO_2 (%) improved compressive strength, and increasing CaO (%) did so only when fly ash replaced 52% to 100% of the cement. For rheological properties, Ferraris and DeLarrard [23] pioneered the study in 2001, focusing on establishing models that link mix composition with rheological properties. In recent years, with the capability of machine learning, Nguyen et al. [24] and Nazar et al. [25] focused on predicting the plastic viscosity of concrete, with the former using Least Squares Support Vector Machine and the latter employing bagging regressor and decision tree, also incorporating yield stress prediction. Mohammed et al. [26] and Nazar et al. [27] explored rheological properties and compressive strength, with the former examining nonlinear regression and neural networks, particularly noting role of nanoclay, and the latter linking raw ingredients of concrete to these properties using gene expression programming. Nazar et al. [28] explored the impact of hydraulic lime on alkali-activated material-based concrete using machine learning and gene expression modeling, uncovering its positive influence on yield stress and plastic viscosity but negative effect on compressive strength, contrasting with fly ash's negative impacts on these properties. Şahin et al. [29] employed Linear Regression Analysis, AdaBoost, and K Nearest Neighbor algorithms to model the rheological properties of cementitious systems, identifying the metakaolin usage ratio as the most influential factor affecting the rheology and thixotropic properties of the mixtures.

Despite numerous data-driven rheological models for conventional concrete, previous studies have focused on only a few materials to derive a regression model for predicting rheological properties. Furthermore, there is a lack of comprehensive study that employs large-scale data mining and machine learning to explore concrete rheology across the literature, especially for the 3DCP sector, aimed at developing a well-suited model specifically for 3DPC.

In the past decade, extensive research has been conducted on rheology and mix design, providing a rich repository of data. It is yet to be determined whether the collection and analysis of this data can lead to the development of new predictive models for the rheology of fresh printed concrete and provide insights into unexplored mix designs.

It is hypothesized that the collected data will support the development of predictive machine learning models that can learn the mapping between the mix designs and their rheological properties. To achieve this, a comprehensive range of 3D printing concrete mix designs is systematically gathered from research results over the last decades. To do this, a predictive model, comprising of only an XGBoost [30] and a Neural Network, was developed to regress on the rheology. Traditionally, pure data-driven models are often criticized for being unexplainable due to their 'black box' nature in making predictions. However, it is essential that researchers and engineers thoroughly understand the model before its reliable application. To address this, we constructed a model explainer, based on the Game Theory - SHapley Additive exPlanations (SHAP) method [31], to interpret the predictions of the developed model. The predictive model helps discover the mapping between the mix design and the rheological behavior, while the explainer justifies the model's prediction.

It is hypothesized that the established predictive model can virtually test new, previously unstudied mix designs and provide valuable insights. To demonstrate its capability, the model was used to predict the rheological properties of sulphoaluminate and clay-based mix designs — a novel family of mix designs that don't exist in the literature. The results indicate that the model is capable of capturing calcined clay's effect on the rheology behavior of sulphoaluminate-based 3D printing concrete, which has not been previously studied by researchers. Moreover, based on the predictive model, we developed a polynomial expression, which is convenient for direct engineering application in designing Portland cement-based 3D printing concrete with varying water to binder ratio and sand to binder ratio. This application is demonstrated in case study, where the polynomial expression is used for estimating rheological properties.

The significance of this study lies in the development of a 3D printing concrete dataset from a decade of literature for the first time, along with a predictive model that can process inputs from nineteen different mix components. This approach surpasses existing rheological models [23–28], which are limited to a few material components as inputs. Furthermore, our model specifically focus on 3DPC, an area previously underexplored in material-to-rheological properties modeling but of critical importance. Moreover, this innovative model has the capability to predict potential new mix designs not yet examined in the literature, opening up novel mix design opportunities for 3DPC, accelerating its research and engineering processes.

2. Rheological Properties of 3D Printing Concrete: Existing Research

Numerous studies have explored the rheological properties of 3D printing concrete through various approaches. Most of such research focuses on exploring binders, aggregates, and admixtures. A selection of representative studies, though not exhaustive, are discussed in this section.

The literature has largely explored the impact of different binders as well as the role of SCMs in concrete. Marchon et al. [32] emphasized the use of various binders and admixtures to adjust the rheological and hydration properties of concrete to meet the demands of the printing process, detailing the necessary concrete properties for each stage, and discussed the types of materials needed to meet these requirements, such as superplasticizers for fluidity during pumping and extrusion, and clays for structural stability during deposition. It also highlights the admixtures that help control setting times and enhance strength gain to ensure successful 3D printing and curing of concrete. In the study of Douba et al. [33], the addition of nanoclays and methylcellulose significantly increased the yield stress of Magnesium oxide paste. Khalil et al. [34] demonstrated that a mix of 7% calcium sulfoaluminate and 93% ordinary Portland cement enhances the rheological behavior and buildability of mortar without compromising its long-term compressive strength. Mohan et al. [10] explored calcium sulfoaluminate cement-based 3D printable concrete, noting that limestone substitution reduces plastic viscosity, and influences buildability. Chen et al. [35] incorporated metakaolin into calcium sulfoaluminate cement composites, which increased the static yield stress and improved thixotropy. The study suggests that controlling thixotropy and yield stress through metakaolin addition can achieve better structural integrity and precision. Chen et al. [36] studied the effect of high substitution of Portland cement with calcined clay and limestone with the same dosage for superplasticizer and viscosity modifying agent (VMA), which improved the buildability of fresh mixs. Panda and Tan [37] and Panda et al. [38] have shown how silica fume, along with ground granulated blast-furnace slag, enhance the rheological properties of mixs, making them suitable for 3D concrete printing. Manikandan et al. [9] found that the addition of silica fume and superplasticizer in cement mixs improves yield stress and maintains viscosity. Similarly, Sikora et al. [39] observed that nanosilica accelerates setting, improves hardening, and rheological properties of mortar, optimizing for 3D printing applications.

Studies on the impact of different aggregates can also be found in the literature. Ting et al. [40] investigated the use of recycled glass as fine aggregates in 3D printable concrete, examining its effects on flow properties, buildability, and mechanical strength, and the necessity of optimizing mix designs for balance between workability and strength. The research by Mohan et al. [41] discussed the effect of varying aggregate to binder ratio in 3D printable cementitious materials, highlighting its significant impact on rheological properties such as plastic viscosity, yield stress, and storage modulus, as well as on printing height and pumping efficiency. The study by Rahul et al. [42] examined the potential of using natural and recycled coarse aggregates in 3D printable concrete, emphasizing the need for adjustments in superplasticizer dosage to maintain yield stress and buildability, and noting improvements in shrinkage and cracking behavior.

The role of admixtures in the rheological properties of 3D printing concrete has also been continuously investigated. Kolawole et al. [43] analyzed how VMA, superplasticizers, and water influence the thixotropic behavior of conventional concrete, with a focus on shearing rate and the pre-history of concrete. Chen et al. [44] highlighted how increasing the dosage of VMA enhances extrudability and shape retention. Chen et al. [45] discussed the improvement in rheological properties necessary for 3D printing, such as extrusion pressure and buildability, by adding VMA. Chen et al. [12] explored the use of hydroxypropyl methyl cellulose, water-reducing agent, and lithium carbonate in sulphoaluminate cement, focusing on its stress and viscosity for 3D printing. The study by Long et al. [13] discussed the addition of micro-crystalline cellulose increasing plastic viscosity and yield stress, enhancing cohesion and printability in sustain-

Table 1
Summary of the collection, standardization, and preprocess steps.

Step	Description
1	**Collect samples**: Select around 90 related papers. Obtain about 500 initial mix design samples.
2	**Standardization**: Normalize binder weight to one. Record other materials as relative percentage to binder. Rename same materials to a uniform name. Obtain the compiled dataset of 500 samples.
3	**Preprocess**: Exclude rare/ambiguous materials before training. Transfer admixtures to ASTM Type A to F, and VMA. Remain 377 samples, 19 material inputs, 3 rheological outputs.

able cement-based composites for 3D printing. Qian and De Schutter [46] compared the efficiencies of Naphthalene Sulfonate Formaldehyde and Polycarboxylate Ether superplasticizers in reducing dynamic yield stress and thixotropy in cement pastes for 3D printing. Chen et al. [47] investigated the effect of tartaric acid on setting time, hydration evolution, and apparent viscosity of sulphoaluminate cement paste for 3D printing.

3. Data Collection and Inspection

To quantitatively analyze the rheological properties of 3D printing concrete, we conducted a comprehensive review of studies in this field over the past decade and compiled a dataset from the literature, including [3, 5, 9–13, 15, 34–112]. The compilation of these papers can be accessed through this link. We standardized the mix designs presented in each paper. This standardization facilitated the training of machine learning models later. Furthermore, we conducted an analysis of the standardized dataset, identifying gaps in the research on 3D printing concrete mix design. Potential research opportunities are highlighted.

3.1. Data Collection and Preprocessing

Table 1 summarizes the processes of data collection, standardization, and preprocessing. Each step is detailed below:

The compiled dataset consists of approximately 500 concrete mix designs for 3D printing. This dataset, collected from about 90 highly relevant studies to printed concrete, represents a broad spectrum of research in this field, including a diverse range of mix designs and the corresponding tests on concrete properties, all methodically collected, cleaned, and uniformly formatted. Those papers were selected inclusively based on their description of detailed mix designs and corresponding experimental results for printed concrete. The dataset has been made publicly available and can be accessed at [113].

A rigorous standardization process was applied to harmonize mix designs from diverse sources. Studies presented mix designs in various formats, including tables and textual descriptions. Quantification methods for material composition varied widely, ranging from volume-based measurements (per cubic meter or yard [114]) to percentages and relative weights. To create a uniform dataset, we meticulously reviewed and standardized each mix design's proportions. Materials with different nomenclatures across studies were assigned consistent terminology. In the final standardized dataset, binder weights were normalized to one, with other components expressed as percentages relative to the binder weight.

Prior to training the models, a preprocess procedure is conducted. Samples with infrequently used (e.g. potassium silicate) or ambiguous materials (e.g non-Polycarboxylate Polymers (PCE) based superplasticizer, non-Hydroxypropyl Methylcellulose (HPMC) based VMA) were excluded, admixture were reviewed and categorized according to the ASTM C494 standard. Type A admixtures, known as water-reducing admixtures, serve to reduce the water requirement of concrete mixs, thereby tending to enhance the workability and strength. Type B, or retarding admixtures, are formulated to delay the setting time of concrete, offering extended workability and placement time. Accelerating admixtures, classified as Type C, are designed to expedite the setting time and early strength development of concrete. Type D admixtures combine the properties of water reduction and setting time retardation, improving both workability and strength of the mix. Type F admixtures, which are high range water-reducing agents, significantly decrease the water content, leading to increased strength and lower permeability. Additionally, the table includes VMA, which are used to adjust the viscosity of the concrete mix. After this step, 377 curated samples remain.

The data preprocess procedure is illustrated in Figure 2. The ingredients are categorized, resulting in 19 distinct categories. The processed data for each mix design sample contains a range of binders including Portland cement, sulfoaluminate cement, fly ash, ground granulated blast-furnace slag, limestone powder, metakaolin, silica fume, diatomite, and calcined clay. The reason to separate metakaolin from general calcined clay is because many papers did not provide the precise type of their calcined clay. The total amount of binder is normalized to one for each sample. Additive admixtures and fibers are also included in the processed data, measured in relative percentage by weight of the binder (%Wob). Each admixture description was reviewed and classified as per ASTM C494 standards. Accordingly, applicable admixtures in each mix design are categorized as ASTM Type A to Type F admixtures. Due to the small number of samples for each type of fiber, we must disregard the type and group them into a single category. While this approach influences the model evaluation of fiber, it is the only feasible solution given the current conditions. Important ratios like the sand to binder and water to binder ratios are formatted. These features serve as the input for the mix design, with the output representing experimental results such as initial Static Yield Stress (kPa), Dynamic Yield Stress (kPa), and Plastic Viscosity (Pa·s).

3.2. Data Inspection

The quantities of the ingredients and experimental results are further examined in Figure 3. Among the final curated 377 mixs, 266 use sand for aggregate, while 111 contain no aggregate. Regarding the binder ingredients, 231 mixs contain Portland cement, followed by 147 containing fly ash, 121 with sulphoaluminate cement, 115 with silica fume, 82 with blast furnace slag, 53 with clay, 44 with diatomite, 41 with limestone, and 14 with metakaolin. In terms of admixtures, Types F admixture and VMA were the most used, featured in 293 and 189 mixs, respectively. Conversely, Types A, B, C, and D were less common, being used in 25, 63, 44, and 34 mixs, respectively. Additionally, 88 mixs contain fibers. For outputs, 178 contains plastic viscosity, 192 contains dynamic yield stress, 142 contains static yield stress.

Three rheological properties for each mix design are included in the data, namely static yield stress, dynamic yield stress, and plastic viscosity. In cases where experimental results are missing from the original literature, they are left empty in the dataset. The intrinsic correlations among rheological properties were investigated using the Pearson correlation coefficient, denoted as $\rho_{X,Y}$. This coefficient is mathematically defined as Equation 2:

$$\rho_{X,Y} = \frac{cov(X,Y)}{\sigma_X \sigma_Y} \tag{2}$$

where $cov(X,Y)$ denotes the covariance between variables X and Y, and σ_X and σ_Y represent their respective standard

Binder	Fly ash:Portland cement:sulphoaluminate cement=0.57:0.4:0.03
Water-Binder Ratio	0.28
Sand-Binder Ratio	0.4
Sand Size (mm)	0-0.3
Admixture(%Wob)	PCE:HPMC=1.2:0.1
Fiber(%Wob)	Polyethylene fiber=1.3
Static Yield Stress (kPa)	11.3
Dynamic Yield Stress (kPa)	0.55
Plastic Viscosity (Pa·s)	11.7

Data Preprocess

Portland cement	0.40
Sulphoaluminate cement	0.03
Fly ash	0.57
Slag	0.00
Limestone powder	0.00
Metakaolin	0.00
Silica fume	0.00
Diatomite	0.00
Clay	0.00
Sand Size Processed (mm)	0.15
Sand-Binder Ratio	0.40
Water-Binder Ratio	0.28
Type A Admixture(%Wob)	0.00
Type B Admixture(%Wob)	0.00
Type C Admixture(%Wob)	0.00
Type D Admixture(%Wob)	0.00
Type F Admixture(%Wob)	1.20
VMA (%Wob)	0.10
Fiber(%Wob)	1.30
Static Yield Stress (kPa)	11.30
Dynamic Yield Stress (kPa)	0.55
Plastic Viscosity (Pa·s)	11.70

Figure 2: Preprocessing of data as model input. Weights of binders are normalized to be one. The water to binder and sand to binder ratios are calculated as the weight ratios relative to the total weight of binders. admixtures and fibers are expressed as weight ratios to the total binder weight, multiplied by 100, and are denoted as %Wob. admixtures are classified to proper types (Type A - F) according to ASTM C494.

deviations.

Consequently, a correlation matrix can be used to show relationships between quantities. A correlation heatmap, which visually represents the correlation matrix, is plotted in Figure 4. It reveals a positive correlation between static yield stress and both dynamic yield stress and plastic viscosity. Conversely, a slight negative correlation is observed between dynamic yield stress and plastic viscosity. The positive correlation between static yield stress and dynamic yield stress is moderate, suggesting some level of association. The positive correlation between static yield stress and plastic viscosity is relatively stronger. It suggests that higher static yield stress is often associated with higher plastic

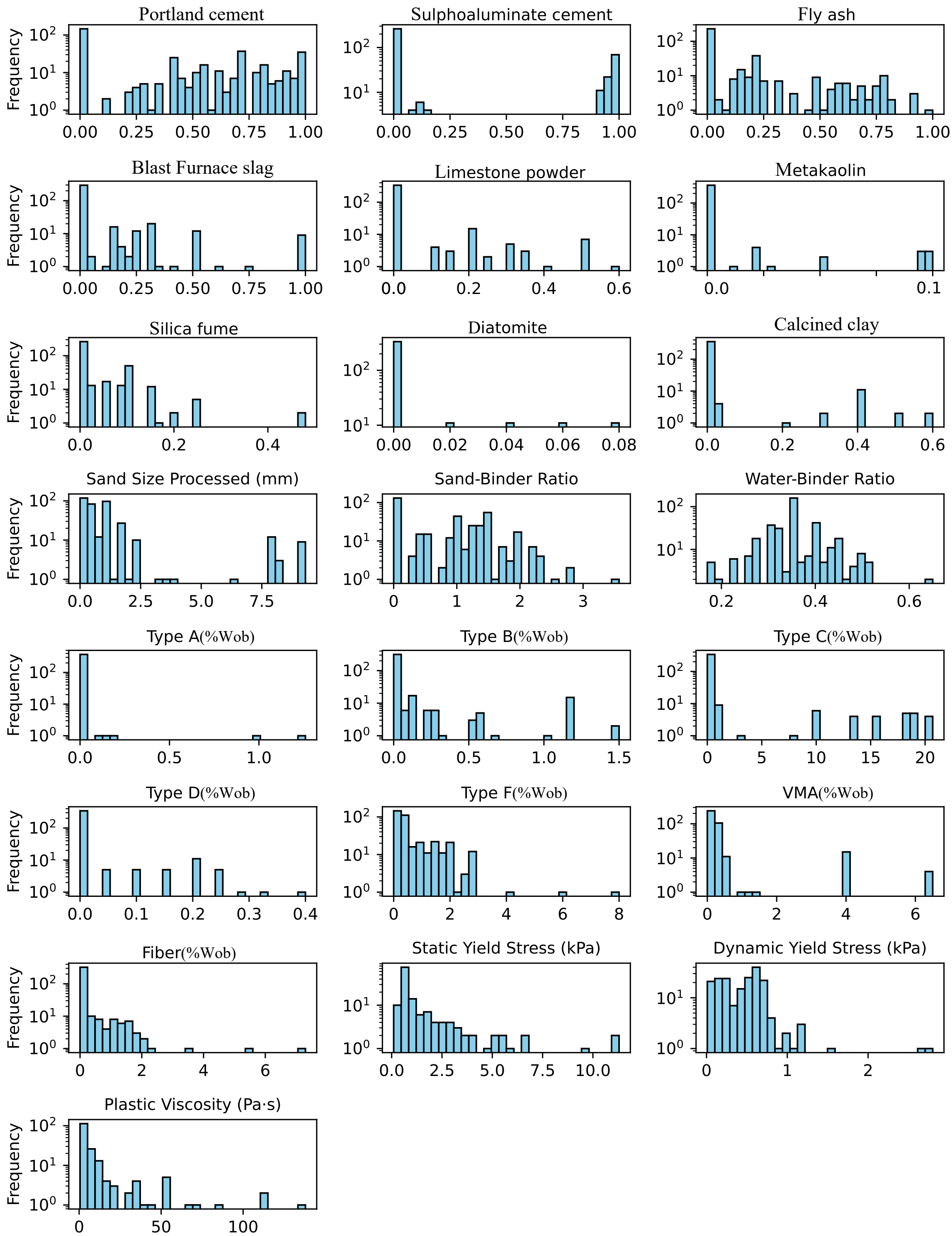

Figure 3: Histogram of feature and property values for selected mix samples. The x-axis represents the numerical values of features and properties, while the y-axis shows the frequency count of each value. The sum of binders, including Portland cement, Sulphoaluminate cement, fly ash, blast furnace slag, limestone powder, metakaolin, silica fume, diatomite, and calcined clay, is normalized to 1. admixtures (Type A to Type F and VMA) and fibers are measured relative to the binder's weight and are represented as a percentage of the binder weight (%wob). The outputs are static yield stress, dynamic yield stress, and plastic viscosity.

viscosity. The negative correlation between dynamic yield stress and plastic viscosity, although weak, indicates that an increase in dynamic yield stress might correspond to a slight decrease in plastic viscosity, or vice versa.

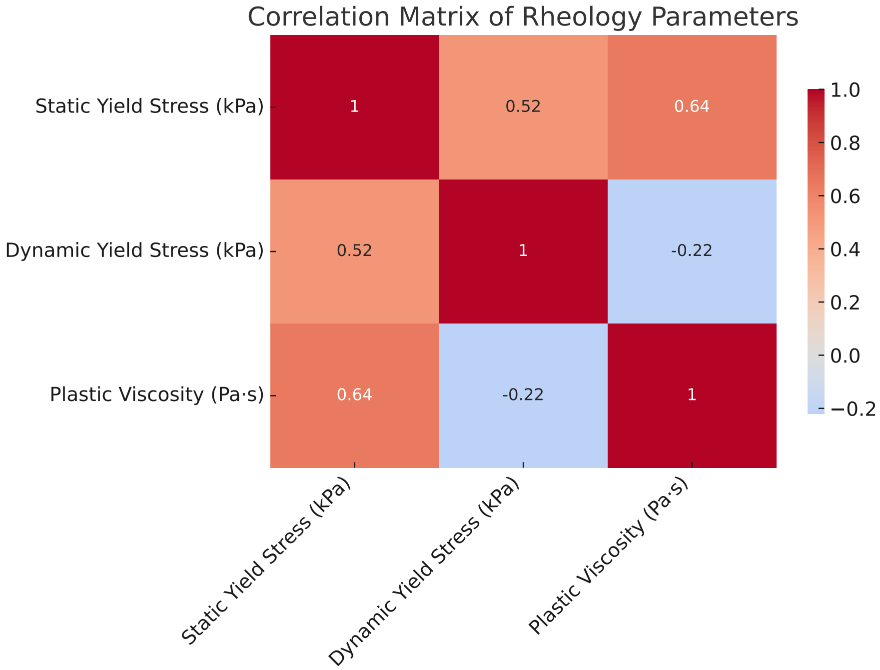

Figure 4: Correlation of the rheological parameters from compiled dataset

3.3. Identified Gaps and Potential Research Opportunities

Based on the inspection of the curated dataset, most binders consist of four or less ingredients, including SCMs. All existing binder designs are listed in Table 2. Combinations not listed in the table present opportunities for novel research. One example is the use of sulphoaluminate cement as the main binder combined with other SCMs, which has been rarely explored, with previous studies only combining it with Diatomite and Metakaolin. Figure 3 presents the frequency histogram of each material count. The proportion of sulphoaluminate cement ranging from 0.2 to 0.8 remains unexplored, indicating a potential area for detailed investigation. In terms of admixtures, the use of Types A, B, C, and D admixtures in binders is an unexplored area. The observed negative correlation between dynamic yield stress and plastic viscosity may suggest the existence of an unexplored intrinsic mechanism. This could mean that a concrete mix with higher dynamic yield stress may exhibit lower plastic viscosity, or vice versa. This observation could indicate a complex interaction between the components of the concrete mix, affecting its flow characteristics, suggesting underlying factors or interactions at the material level that are not fully understood yet. It indicates a potential area for

Table 2
Categorization of 3D printing concrete binders over the past decade. This table encompasses the primary combinations explored in recent research. Binder combinations not represented here may constitute unexplored areas, presenting potential opportunities for pioneering research.

Category	Count	Binder
One binder	55	Sulphoaluminate Cement
	27	Portland Cement
	9	Blast Furnace Slag
	1	Fly Ash
Portland Cement + 1 SCM	19	Portland Cement, Fly Ash
	13	Portland Cement, Sulphoaluminate Cement
	12	Portland Cement, Blast Furnace Slag
	10	Portland Cement, Silica Fume
	6	Portland Cement, Limestone Powder
	5	Portland Cement, Calcined Clay
Portland Cement + 2 SCMs	49	Portland Cement, Fly Ash, Silica Fume
	21	Portland Cement, Fly Ash, Blast Furnace Slag
	9	Portland Cement, Fly Ash, Calcined Clay
	4	Portland Cement, Fly Ash, Limestone Powder
	3	Portland Cement, Fly Ash, Sulphoaluminate Cement
	18	Portland Cement, Limestone Powder, Calcined Clay
	4	Portland Cement, Limestone Powder, Silica Fume
	5	Portland Cement, Blast Furnace Slag, Silica Fume
	2	Portland Cement, Blast Furnace Slag, Limestone Powder
	5	Portland Cement, Silica Fume, Metakaolin
	1	Portland Cement, Silica Fume, Calcined Clay
Portland Cement + 3 SCMs	9	Portland Cement, Fly Ash, Silica Fume, Calcined Clay
	4	Portland Cement, Metakaolin, Silica Fume, Calcined Clay
	3	Portland Cement, Sulphoaluminate Cement, Fly Ash, Calcined Clay
	2	Portland Cement, Limestone Powder, Metakaolin, Silica Fume
Sulphoaluminate Cement Based	44	Sulphoaluminate Cement, Diatomite
	3	Sulphoaluminate Cement, Metakaolin
Fly Ash Based	3	Fly Ash, Blast Furnace Slag
	1	Fly Ash, Silica Fume
	21	Fly Ash, Blast Furnace Slag, Silica Fume
	4	Fly Ash, Blast Furnace Slag, Silica Fume, Calcined Clay
Blast Furnace Slag Based	5	Blast Furnace Slag, Limestone Powder

further research to understand the fundamental principles governing these properties. Such understanding could lead to the development of more advanced models for predicting concrete behavior and could have practical applications in improving concrete mix design.

4. Predictive Model and Phenomenological Explanation

4.1. Predictive Model

With the data, we aim to develop regression models to predict dynamic yield stress, static yield stress, and plastic viscosity separately with given mix design information. The models are pure data-driven. It would be convenient to use such models for analyzing existing mix designs and exploring new designs without experiments. There are numerous algorithms to be chosen from. Among those, XGBoost, a gradient-boosted tree-based model, usually excels with smaller datasets like ours. However, it tends to overfit the data, and is sensitive to noise and minor fluctuations in the training data. Additionally, the interpolation and extrapolation (generalization) performance of XGBoost is usually found to be suboptimal. In contrast, neural networks are good at capturing nonlinear patterns in the data, while there is a concern about its ability to generalize across the entire range of the data, especially for cases where data might be sparse and small. To leverage the strengths of both approaches, we applied ensemble models that integrate XGBoost and NeuralNet as submodels. Each submodel is independently trained on the same dataset to produce initial predictions. These predictions are then concatenated with the original input features, forming an enriched dataset. This enriched dataset serves as input for second-layer models. The optimal configurations of multi-layer stacking are determined by selecting some best combinations, allowing the ensemble model to combine the predictive capabilities of XGBoost and Neural Networks. Further details about the concept of the ensemble technique are beyond the scope of this research, but interested readers are referred to the original paper of this method [115].

To demonstrate the advantages of the predictive ensemble model, we set up an example case, where the sand size is 1.0 mm, the sand to binder ratio is 1.0, and the water to binder ratio is 0.4. Then, based on this setup, the model is used to predict the dynamic yield stress of pure Portland cement-based concrete varies with VMA content. As shown in Figure 6, the XGBoost model's zigzaggy prediction pattern indicates possible overfitting, despite of its inherent nature of decision trees in capturing binary splits. The NeuralNet prediction is smooth, but its accuracy within the sample domain is not as good as the XGBoost model when tested on our data. The ensemble model leverages the distinct strengths of both models: the XGBoost regressor excels in the efficient capturing of feature interactions, while the neural network excels in modeling complex, non-linear relationships. The combination addresses the individual limitations observed when they were used separately. Specifically, the neural network's ability to produce smooth

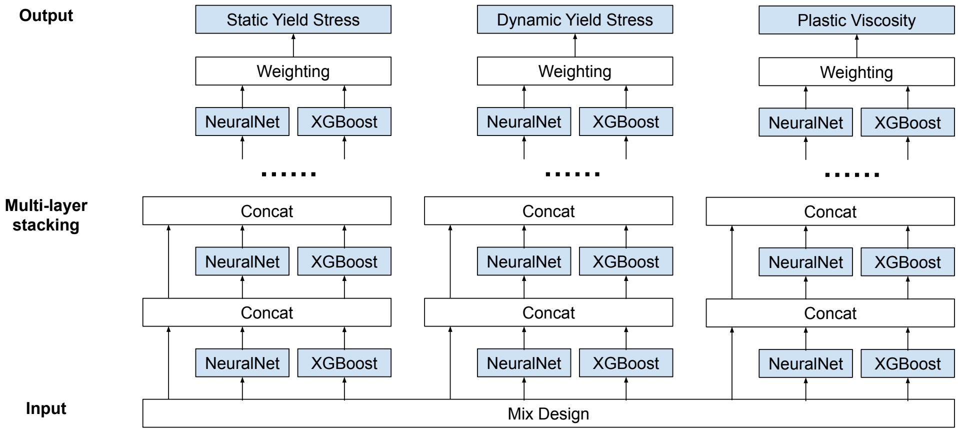

Figure 5: Multi-layer stacking ensemble model structure.

predictions complements the XGBoost model's precision in data interpretation, leading to a more robust and accurate model overall.

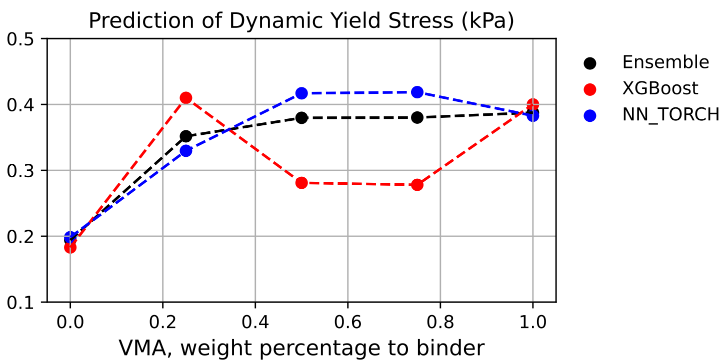

Figure 6: Comparison of Ensemble model, XGBoost and Neural network, on Portland cement concrete with 1mm sand size, 1.0 sand to binder ratio and 0.4 water to binder ratio

The trained ensemble model is then evaluated on a test dataset, resulting R-squared (R^2) values are 0.917, 0.908, and 0.959 for static yield stress, dynamic yield stress, and plastic viscosity, respectively. R^2 is the performance metric calculated using the Equation 3:

$$R^2 = 1 - \frac{\sum_i (y_i - \hat{y}_i)^2}{\sum_i (y_i - \bar{y})^2} \tag{3}$$

where y_i is the actual value, $\hat{y}_i$ is the predicted value, and $\bar{y}$ is the mean of the actual values.

The model's performance is further illustrated in Figure 7, with the ground truth values plotted on the x-axis and predicted values on the y-axis. There is a significant alignment between the predicted and ground truth values, underscoring the model's capability in capturing the pattern of the data. This high degree of alignment between predictions and ground truth emphasizes the model's robustness and reliability in practical applications.

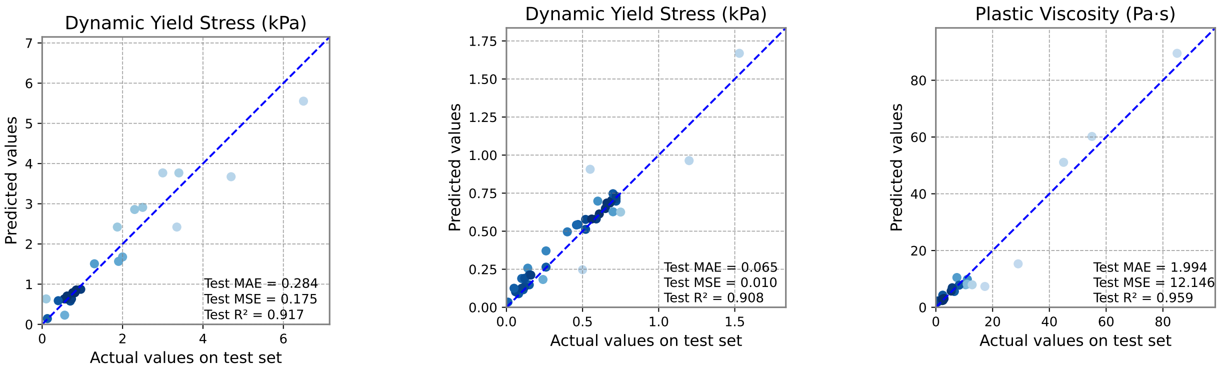

(a) Static Yield Stress (b) Dynamic Yield Stress (c) Plastic Viscosity

Figure 7: Model performance of the Ensemble model on the test dataset

4.2. A Game-Theoretical Approach to Model Interpretation

Regression models, especially in complex tasks like concrete mix rheology prediction, often act as 'black boxes', offering predictions without clear explanations. The lack of transparency can make them less trustworthy for practical use. To address this issue, it is essential to understand how these models arrive at their decisions.

To achieve this, we employ SHapley Additive exPlanations (SHAP) [31], a methodological framework for interpreting machine learning models. SHAP is developed on the concept of Shapley values from the cooperative game theory, where they serve as a metric for 'feature importance' in a machine learning model. In this context, the Shapley value concept is adapted to quantify the contribution of each feature (i.e., input variable) to a specific prediction of a model. This approach enables the understanding of how each input factor influences the model's output.

For a given feature, a SHAP value quantifies its impact on the model's prediction comparatively to a baseline scenario, where the feature assumes an average value. The Shapley value for a feature is mathematically formulated as:

$$\phi_i = \sum_{S \subseteq N \setminus \{i\}} \frac{(|S|)!(n - |S| - 1)!}{n!} \left(v(S \cup \{i\}) - v(S)\right) \tag{4}$$

where, ϕ_i represents the Shapley value for a particular feature, designated as feature i. The term N stands for the total set of features included in the model. The subset S refers to any subset of features that does not include feature i. This approach is employed to assess the contribution of feature i in various combinations with other features. The function $v(S)$ indicates the predicted output of the model when it considers only the features included in subset S. Essentially, the equation calculates the average contribution of feature i across all possible combinations of features, offering an understanding of impact of input on the output.

The computation of SHAP values employs the Kernel SHAP method, a weighted linear regression technique designed to estimate these values for any model. This is represented by the equation:

$$\hat{\phi} = \underset{\phi}{\operatorname{argmin}} \sum_{S \subseteq N} \left[f_x(S) - \phi_0 - \sum_{i \in S} \phi_i \right]^2 \omega(S), \tag{5}$$

where $\hat{\phi}$ denotes the estimated SHAP values, $f_x(S)$ is the model output for a subset of features S, ϕ_0 is the baseline output, and $\omega(S)$ is the weight attributed to each subset S.

Through SHAP analysis, we can discern the individual contribution of each input to a prediction, thereby quantifying the internal dynamics of the model's predictions. Moreover, analyzing the mean of absolute Shapley values for a feature across all samples leads to the understanding of the feature's overall impact on the model.

4.3. Feature Selection and Data Generation

To perform the model explanation, we need to select input features to be explained, and then generate data of these features. The explanation will then be based on the generated data. Six common features were selected for the explanation: 'Portland Cement', 'Sulphoaluminate Cement', 'Fly Ash', 'Silica Fume', 'Type F', 'VMA'. The first four features belong to the binders/SCMs category. Given the limited number of samples and the sparsity of representation in the original dataset, additional sampling was performed to augment the data and facilitate the explanation of selected features. Considering their original distribution, Dirichlet distribution was used for joint sampling. Because it effectively models the proportions of the binders and SCMs, ensuring they sum to 1. This distribution provides a straightforward method to incorporate prior knowledge about the mix design proportions. Based on the observed coverage of binders in the dataset, a Dirichlet distribution with alpha parameters [1, 1, 1, 0.5] was employed to encompass the design space of the four binders. Expression of Dirichlet distribution dense function is shown as Equation 6. The VMA and Type F were sampled by uniform distribution between 0 to 5. Other features such as the water to binder ratio, sand to binder ratio, sand size were kept consistent at 0.40, 1.0, and 1.0 mm, separately. And all other ingredients were set to zero. Figure 8 shows the histogram of sampled data for SHAP interpretation.

$$f(\boldsymbol{X};\boldsymbol{\alpha}) = \frac{1}{B(\boldsymbol{\alpha})}\prod_{i=1}^{k} x_i^{\alpha_i-1} \tag{6}$$

where $\boldsymbol{X} = [x_1, x_2, \ldots, X_k]$ is a vector of probabilities with k components, $\boldsymbol{\alpha} = [\alpha_1, \alpha_2, \ldots, \alpha_k]$ is the vector of concentration parameters for the Dirichlet distribution, and $\boldsymbol{B}(\boldsymbol{\alpha})$ is the multinomial beta function, which serves as a normalization constant to ensure that the total probability integrates to 1.

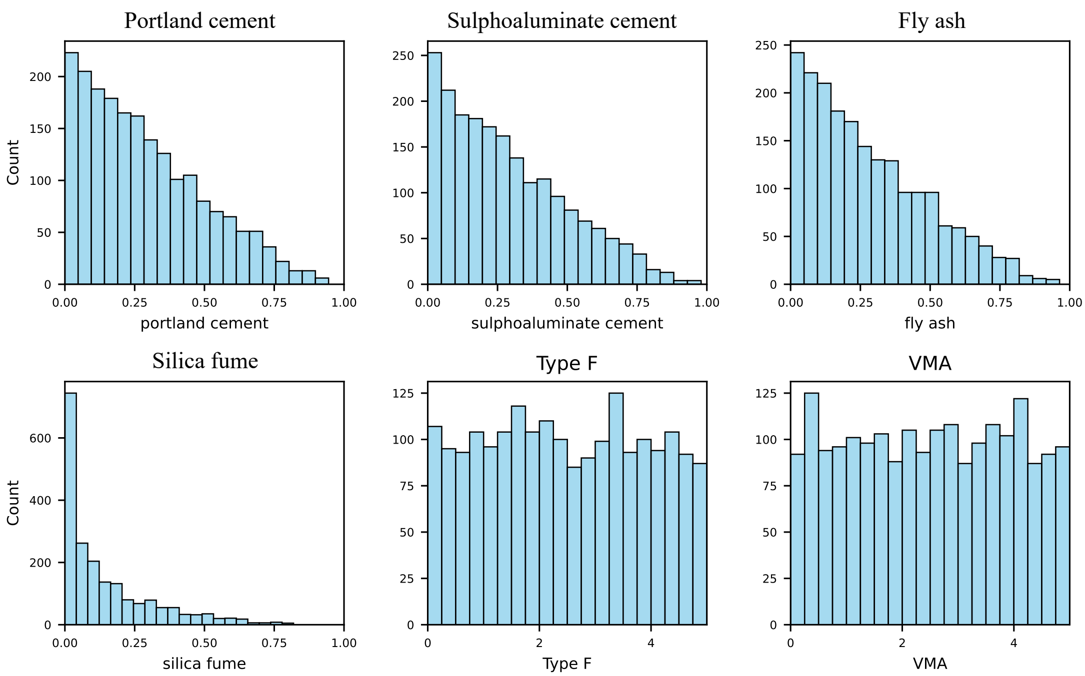

Figure 8: Histogram of sampled data for selected features. Portland cement, sulphoaluminate cement, fly ash, and silica fume are sampled by Dirichlet distribution with alpha parameters [1.0, 1.0, 1.0, 0.5]. Type F admixture and VMA are sampled by even distribution.

4.4. Explanation of the Trained Model

The SHAP result of each ingredient is then demonstrated using the beeswarm plots in Figure 9, Figure 10, and Figure 11 for static yield stress, dynamic yield stress, and plastic viscosity, respectively. In those figures, red means the feature value is larger than average, blue means the feature value is lower than average. When the SHAP value is positive, it means the corresponding feature value has a positive impact on the final prediction. When the SHAP value is negative, it indicates the corresponding feature value would have negative impact on the prediction. In the beeswarm plots, a higher position of a feature corresponds to a higher mean absolute SHAP value for that feature, which can approximately be regarded as the 'overall importance rank' of that feature. The changes in the top features would cause more significant changes in the rheological characteristics of concrete.

Figure 9 displays a SHAP summary plot detailing the influence of various factors on the static yield stress, measured in kPa. For binders, Portland cement percentage significantly impacts the static yield stress, exhibiting a complex and non-linear relationship that can either reduce or augment the stress under certain conditions. Silica fume appears to slightly enhance the static yield stress under some conditions, while sulphoaluminate cement, fly ash, VMA and Type F admixture may not significantly impact static yield stress.

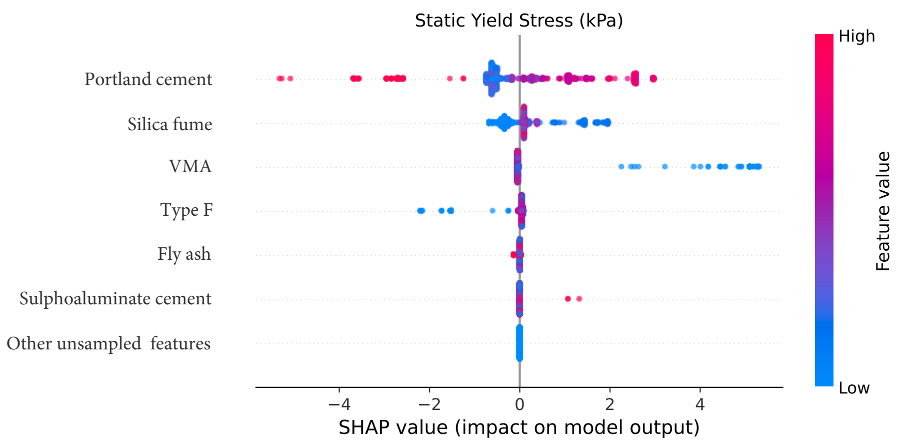

Figure 9: SHAP result: static yield stress

Figure 10 illustrates the impact of various elements on the dynamic yield stress, also measured in kPa. The percentage of Portland cement, sulphoaluminate cement, and fly ash in binders all negatively affects the dynamic yield stress, while silica fume seems to improve the dynamic yield stress. VMA and Type F admixture both stand out as the most influential. A higher content of them is associated with a possible rise in dynamic yield stress.

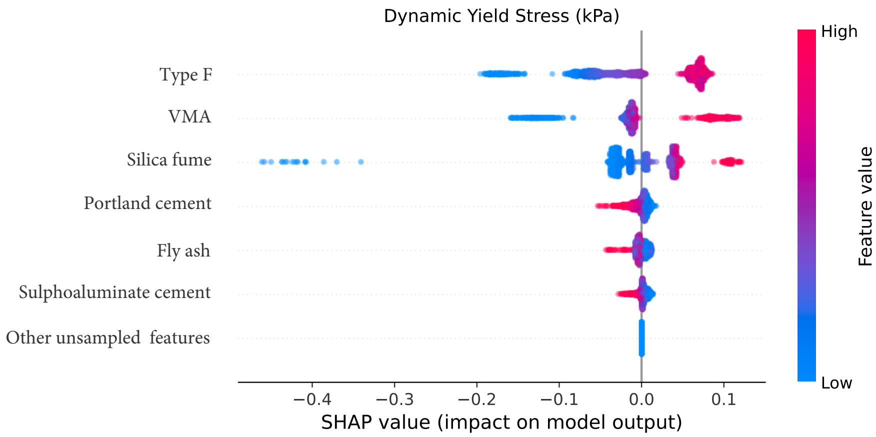

Figure 10: SHAP result: dynamic yield stress

Figure 11 demonstrates the influence on plastic viscosity, expressed in Pa.s. In terms of binders, fly ash would increase the plastic viscosity, while silica fume reduces the plastic viscosity. Portland cement and sulphoaluminate cement have little influence. For admixtures, Type F admixture reduces the plastic viscosity, while VMA increases it.

The SHAP-identified impacts of various inputs on rheological properties are summarized in Table 3.

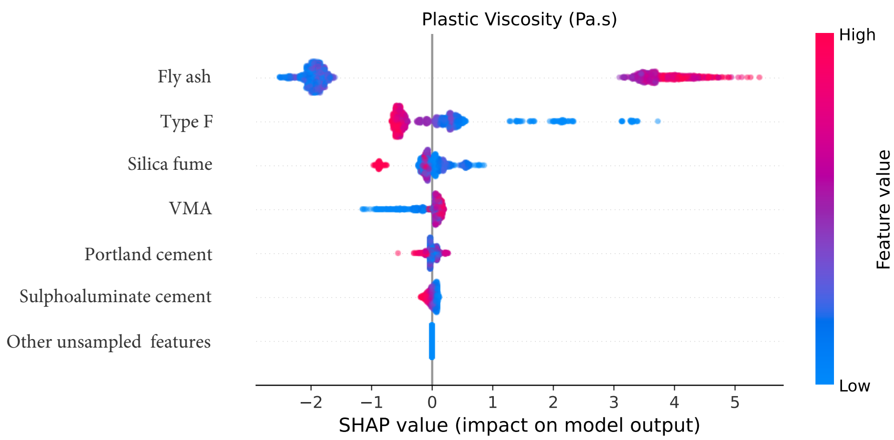

Figure 11: SHAP result: plastic viscosity

5. Prediction on Unexplored Mix Designs

As indicated in Table 2, the combination of sulphoaluminate cement with calcined clay in printed concrete has not been previously well-explored in the collected literature. Using this combination as an example, we demonstrate the

Table 3
Summary of SHAP value influences on printing concrete properties for major SCMs and admixtures

Factor	Static Yield Stress (kPa)	Dynamic Yield Stress (kPa)	Plastic Viscosity (Pa.s)
Portland Cement	Significant	Reduces	Not significant
Silica Fume	May slightly increases	Increases	Reduces
Sulphoaluminate Cement	Not significant	Slightly reduces	Not significant
Fly Ash	Not significant	Slightly reduces	Increases
VMA	Not significant	Increases	Increases
Type F admixture	Not significant	Increases	Reduces

potential of our method for predicting on unexplored mix designs. Based on this combination, we developed a series of mixs by varying the variables of the mix design. The variables include Type D admixture ranging from 0% to 0.25% of binder weight, Type F admixture fixed at 0.3%, VMA set at 0.4%, calcined clay from 0.02% to 0.08% and a water to binder ratio of 0.35. Those values are chosen based on a printed concrete paper using sulphoaluminate cement without calcined clay [75]. Our developed model is used for making predictions on the static yield stress of mix designs of this range.

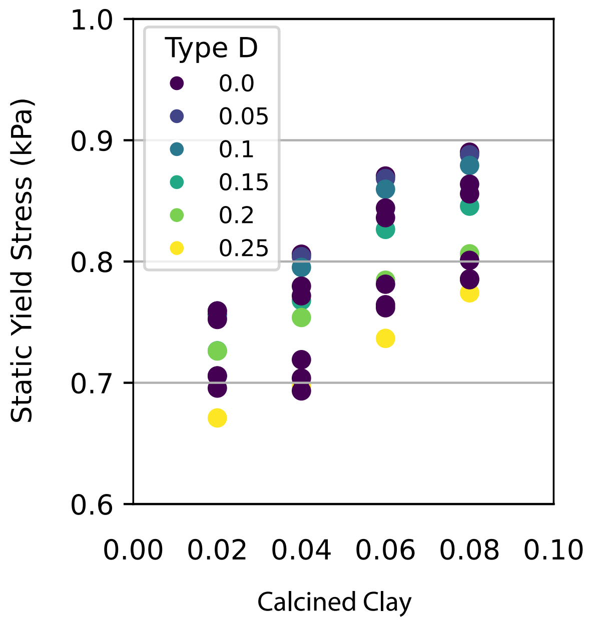

Figure 12: Prediction of Static Yield Stress in sulphoaluminate-based concrete with clay. This illustrates the trained model is able to predict properties of mix designs outside the dataset.

As shown in Figure 12, the plot illustrates the predicted static yield stress of sulphoaluminate cement-based concrete combined with calcined clay. The model shows that adding calcined clay to sulphoaluminate cement paste would increase the static yield stress within this range.

To verify such a prediction, the actual impact of adding calcined clay to sulphoaluminate cement paste should be empirically tested. The exact qualitative result could also depend on the specific types of calcined clay and sulphoaluminate cement used, as well as the proportions and other components of the concrete mix.

6. Discussions

6.1. Explicit Equations

Compared to the predictive ensemble model, explicit equations such as polynomial expressions are intrinsically interpretable and convenient for engineering applications. But they are not easy to be developed from relatively small but highly non-linear dataset. In this section, we show examples of developing such expressions using the trained ensemble model from the previous section. Based on observation of outputs, we define polynomial equations. The parameters of the equations are then fitted by the data generated from the ensemble model. Alternative forms of functions are possible. However, we aim to keep a balance between simplicity and accuracy.

In the first example, we examine a typical Portland cement-based concrete, characterized by a sand to binder ratio of 1.0 and an average sand size of 1.0 mm. This scenario includes the use of VMA and Type F admixtures, varying from 0 to 1 percent weight of binder, along with an adjustable water to binder ratio that ranges from 0.15 to 0.65. The results of the polynomial regression for this case are presented in Equation 7 and illustrated in Figure 13.

$$
\begin{aligned}
\text{Static Yield Stress} &= 1.16 - 0.55x_1 + 0.39x_1^2 + 0.17x_2 - 0.30x_3 \,\text{kPa} \\
\text{Dynamic Yield Stress} &= 0.33 - 0.27x_1 - 0.16x_1^2 + 0.08x_2 + 0.19x_3 \,\text{kPa} \\
\text{Plastic Viscosity} &= 6.85 + 1.07x_1 - 3.77x_1^2 - 0.72x_2 + 1.10x_3 \,\text{Pa·s}
\end{aligned}
\tag{7}
$$

where x_1 represents the water to binder ratio, x_2 is the weight percentage of Type F relative to the binder, and x_3 denotes the VMA weight percentage of the binder. These equations are specifically formulated for Portland cement-based 3D printing concrete with a sand to binder ratio of 1.0, an average sand size of 1.0 mm, excluding all other SCMs and admixtures.

In the second example, we focus on Portland cement-based concrete with a water to binder ratio of 0.4 and an average sand size of 1.0 mm. This example assumes the inclusion of VMA and Type F admixtures, varying from 0 to 1 percent, while the sand to binder ratio varies from 0 to 3.0. The polynomial regression results for this scenario are presented in Equation 8, and are illustrated in Figure 13.

$$
\begin{aligned}
\text{Static Yield Stress} &= 1.01 - 0.46x_1 + 0.56x_1^2 + -0.12x_1^3 + 0.17x_2 - 0.31x_3 \text{ kPa} \\
\text{Dynamic Yield Stress} &= 0.19 + 0.01x_1 + 0.08x_2 + 0.19x_3 \text{ kPa} \\
\text{Plastic Viscosity} &= 5.26 + 39.42\frac{1}{1+e^{-20(x_1-1.7)}} - 0.05x_2 + 1.15x_3
\end{aligned} \tag{8}
$$

where x_1 represents the sand to binder ratio, x_2 is the weight percentage of Type F relative to the binder, and x_3 denotes the VMA weight percentage of the binder. These equations are specifically formulated for Portland cement-based 3D printing concrete with a water to binder ratio of 0.4, an average sand size of 1.0 mm, excluding all other SCMs and admixtures.

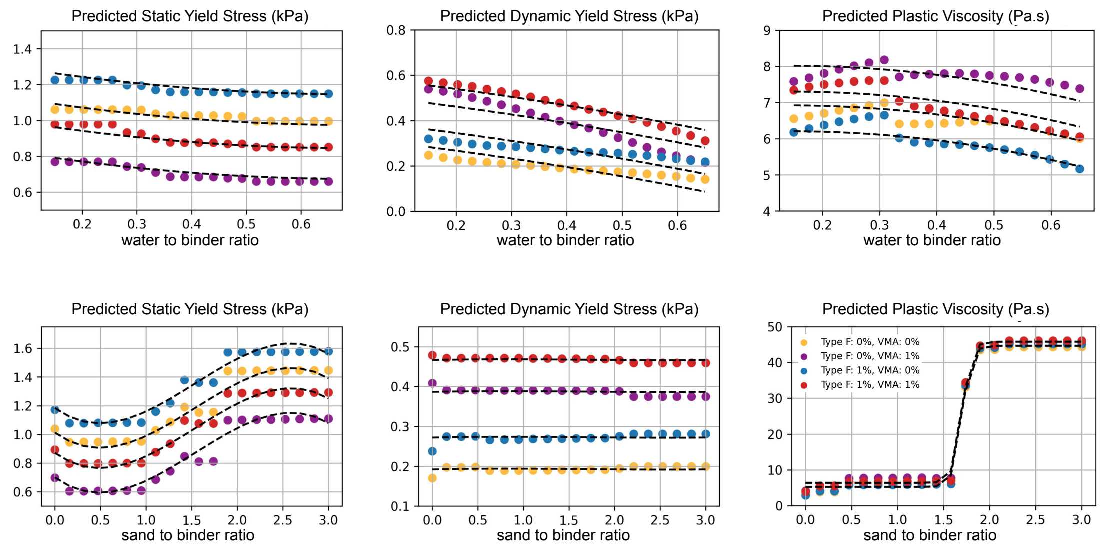

Figure 13: Regression plot of rheological parameters vary with water to binder ratio (top), and vary with sand to binder ratio (bottom), based on the polynomial expressions provided in Equation 7 and Equation 8. Scatters are derived from the ensemble models.

6.2. Further Discussions

The presented results are based on a dataset collected from a decade of research in 3D printing concrete. The dataset is a compilation of 3D printing mix designs and rheological experiments. Despite the differences in the testing systems (e.g., testing time, experimental method, equipment condition, testing environment, and potential human errors), the data has been standardized into a consistent format based on expert judgment. While the noise and uncertainties in the data should be acknowledged, they are not explicitly quantified in this study, as they fall outside its primary focus.

Based on the dataset, we developed a predictive ensemble model, which is aimed at evaluating the rheological properties of various concrete mix designs. This model integrates two algorithms (XGBoost and NeuralNet), leveraging the strengths of each to predict concrete properties with balanced accuracy and generalizability.

To ensure the transparency and interpretability of the model, we utilized SHAP to explain the predictions of the model. SHAP is a robust framework for understanding the contribution of each input to the output of the model, thereby enhancing the clarity of our predictive model. However, there are certain limitations in SHAP-based explainers. The effectiveness and accuracy of SHAP's explanations are highly dependent on the quality and representativeness of the data being explained. In scenarios where the data is sparse or unrepresentative of the broader context, SHAP values might not accurately capture the full impact of certain parameters on the rheological properties. This could lead to incomplete or skewed interpretations of how different factors influence the predictions of the model.

In the context of the present study, certain features in our data is sparse. This causes difficulty for the SHAP explainer when evaluating contributions of certain parameters. To mitigate this issue, we enhanced the data with sampled mix designs by Dirichlet and uniform distributions. By doing so, we aimed to feed an enhanced and balanced dataset to the model, which could improve the effectiveness of SHAP's explanations. However, it is important to remain cautious about the potential limitations of SHAP in interpreting the effects of certain parameters, especially when dealing with complex and multifaceted rheological properties. We suggest applying and interpreting predictive models with a critical and informed perspective.

One advantage of a predictive model is its capability to predict the behavior of untested, novel mix designs. This is particularly valuable in concrete research, because the development of new mix designs is usually costly and time-consuming. By learning from historical data, the model can predict the properties of mixs that have not yet been physically created/tested. This can significantly accelerate the mix design process, enabling rapid innovation and optimization.

Based on our ensemble model, we demonstrated the derivation of explicit polynomial expressions. Similar to the ensemble model, the explicit expressions can be used for predicting the rheological properties of concrete mixs. Compared to the ensemble model, the explicit expressions are naturally interpretable and convenient for practical engineering applications. We showed two examples with varying mix design parameters (sand to binder ratio and different admixtures). There could be alternative forms of equations, some of which may be very complex. However, we aim to balance simplicity and accuracy, so we chose low-order polynomial terms to construct the equations. This approach still shows sufficient accuracy.

This study makes contributions through both its comprehensive dataset and innovative models. The dataset advances the field by enabling a data-driven approach to mix design complexities. Analysis of this dataset yields valuable insights into printed concrete mix design and reveals potential research gaps. For practitioners looking to design their printed concrete, the dataset serves as a valuable reference offering access to recorded mix designs that can guide and inform their projects. With the models, practitioners can virtually test their designs. This would allow them to explore novel mix designs rapidly.

It is noteworthy that our model simplifies the complex rheology of fresh concrete by averaging variations in ingredients, environments, and testing methods, and by treating concrete as a homogeneous fluid with constant properties, ignoring time-dependent hydration reactions. While this approach aligns with existing models, it may not capture all nuances. Users should interpret results cautiously, especially in sensitive designs requiring precise rheological control. Future research could benefit from larger, more detailed datasets to improve model accuracy and applicability.

7. Conclusion

Additive construction with concrete is an emerging sector that faces significant challenges in designing optimal mixes for various projects, given the precision and unique rheological properties required. Recognizing the potential of data in addressing these challenges, numerous studies have relied on small, isolated datasets. However, a large, comprehensive dataset in this field has remained elusive. Inspired by the ImageNet dataset, which served as the catalyst for the current wave of advancements in artificial intelligence, we are among the first to develop a comprehensive additive construction concrete dataset, which is continuously expanding. This dataset aims to address the complexities of mix design through a data-driven approach.

1. A dataset of ~500 samples has been compiled from 3D printed concrete research of the last decade. In 3D printing concrete, Portland cement remains the predominant binder, featuring in 231 of the surveyed mix designs. Other common binders/SCMs include fly ash (147 designs), sulphoaluminate cement (121 designs), and silica fume (115 designs). Among admixtures, Type F superplasticizer and VMA were most frequently utilized, appearing in 293 and 189 mixes, respectively.
2. The curated dataset reveals a notable lack of case studies where sulphoaluminate cement comprises 20% to 80% of the total binder. The potential of sulphoaluminate cement as the primary binder in combination with other SCMs, remains underexplored.
3. The tailored ensemble model, which combines XGBoost and Neural Networks, demonstrated high performance in predicting the rheological properties of 3D printing concrete, achieving R^2 values of 0.917, 0.908, and 0.959 on the test dataset. After SHAP analysis, this model is not a black box but interpretable. The relative SHAP results of various components provide references to adjust the mix proportions, helping optimizing the rheological properties of the concrete. This enhanced transparency increases practicality and reliability.
4. The predictions of unexplored mix designs using the developed models suggest that, within specific ranges, the addition of calcined clay in sulphoaluminate cement paste could potentially lead to a higher static yield stress. Furthermore, the trained machine learning model has been distilled into explicit polynomial expressions, offering engineers and practitioners a transparent, rapid, and computationally efficient tool for real-world applications.

Continuously expanding and enriching the dataset will be a key aspect of future work. The dataset should be continuously updated with new concrete mix designs and experimental results. Each new entry shall be manually verified against original sources for accuracy. The dataset should be enriched with more detailed mix parameters, experimental conditions, and expanded result metrics. This research establishes a foundation for applying data-driven models to streamline the mix design process for additive construction concrete, ultimately contributing to more efficient and cost-effective practices in mix design.

Acknowledgments

This work was supported by the National Science Foundation under Grant No. 2235678. This work was also performed under the auspices of the U.S. Department of Energy by Lawrence Livermore National Laboratory under Contract DE-AC52-07NA27344.

References

[1] Freek Bos, Rob Wolfs, Zeeshan Ahmed, and Theo Salet. Additive manufacturing of concrete in construction: potentials and challenges of 3d concrete printing. *Virtual and Physical Prototyping*, 11(3):209–225, 2016.

[2] Geert De Schutter, Karel Lesage, Viktor Mechtcherine, Venkatesh Naidu Nerella, Guillaume Habert, and Isolda Agusti-Juan. Vision of 3D printing with concrete—Technical, economic and environmental potentials. *Cement and Concrete Research*, 112:25–36, 2018.

[3] Biranchi Panda and Ming Jen Tan. Experimental study on mix proportion and fresh properties of fly ash based geopolymer for 3D concrete printing. *Ceramics International*, 44(9):10258–10265, 2018.

[4] Nicolas Roussel. Rheological requirements for printable concretes. *Cement and Concrete Research*, 112:76–85, 2018.

[5] Yiwei Weng, Mingyang Li, Ming Jen Tan, and Shunzhi Qian. Design 3D printing cementitious materials via Fuller Thompson theory and Marson-Percy model. *Construction and Building Materials*, 163:600–610, 2018.

[6] Chao Zhang, Venkatesh Naidu Nerella, Anurag Krishna, Shen Wang, Yamei Zhang, Viktor Mechtcherine, and Nemkumar Banthia. Mix design concepts for 3D printable concrete: A review. *Cement and Concrete Composites*, 122:104155, 2021.

[7] Delphine Marchon, Shiho Kawashima, Hela Bessaies-Bey, Sara Mantellato, and Serina Ng. Hydration and rheology control of concrete for digital fabrication: Potential admixtures and cement chemistry. *Cement and Concrete Research*, 112:96–110, 2018.

[8] Shiho Kawashima, Kejin Wang, Raissa Douglas Ferron, Jae Hong Kim, Nathan Tregger, and Surendra Shah. A review of the effect of nanoclays on the fresh and hardened properties of cement-based materials. *Cement and Concrete Research*, 147:106502, 2021.

[9] Karthick Manikandan, Kwangwoo Wi, Xiao Zhang, Kejin Wang, and Hantang Qin. Characterizing cement mixtures for concrete 3D printing. *Manufacturing Letters*, 24:33–37, 2020.

[10] Manu K Mohan, AV Rahul, Geert De Schutter, and Kim Van Tittelboom. Early age hydration, rheology and pumping characteristics of CSA cement-based 3D printable concrete. *Construction and Building Materials*, 275:122136, 2021.

[11] Jeong Su Kim, Seung Hee Kwon, Kyong Pil Jang, and Myoung Sung Choi. Concrete pumping prediction considering different measurement of the rheological properties. *Construction and Building Materials*, 171:493–503, 2018.

[12] Mingxu Chen, Laibo Li, Yan Zheng, Piqi Zhao, Lingchao Lu, and Xin Cheng. Rheological and mechanical properties of admixtures modified 3D printing sulphoaluminate cementitious materials. *Construction and Building Materials*, 189:601–611, 2018.

[13] Wu-Jian Long, Jie-Lin Tao, Can Lin, Yu-cun Gu, Liu Mei, Hua-Bo Duan, and Feng Xing. Rheology and buildability of sustainable cement-based composites containing micro-crystalline cellulose for 3D-printing. *Journal of Cleaner Production*, 239:118054, 2019.

[14] Geoffrey Howarth Tattersall and Phillip FG Banfill. *The rheology of fresh concrete*. 1983.

[15] Yu Zhang, Yunsheng Zhang, Wei She, Lin Yang, Guojian Liu, and Yonggan Yang. Rheological and harden properties of the high-thixotropy 3D printing concrete. *Construction and Building Materials*, 201:278–285, 2019.

[16] I-C Yeh. Modeling of strength of high-performance concrete using artificial neural networks. *Cement and Concrete research*, 28(12): 1797–1808, 1998.

[17] Y Song, B Ouyang, J Chen, X Wang, K Wang, S Zhang, Y Chen, G Sant, and M Bauchy. Decarbonizing concrete with artificial intelligence. In *Computational Modelling of Concrete and Concrete Structures*, pages 168–176. CRC Press, 2022.

[18] Wael Emad, Ahmed Salih Mohammed, Rawaz Kurda, Kawan Ghafor, Liborio Cavaleri, Shaker M.A.Qaidi, A.M.T. Hassan, and Panagiotis G. Asteris. Prediction of concrete materials compressive strength using surrogate models. *Structures*, 46:1243–1267, 2022.

[19] Hemn Unis Ahmed, Ahmed S Mohammed, Rabar H Faraj, Aso A Abdalla, Shaker MA Qaidi, Nadhim Hamah Sor, and Azad A Mohammed. Innovative modeling techniques including MEP, ANN and FQ to forecast the compressive strength of geopolymer concrete modified with nanoparticles. *Neural Computing and Applications*, 35(17):12453–12479, 2023.

[20] Hamed Naseri, Pardis Hosseini, Hamid Jahanbakhsh, Payam Hosseini, and Amir H Gandomi. A novel evolutionary learning to prepare sustainable concrete mixtures with supplementary cementitious materials. *Environment, Development and Sustainability*, 25(7):5831–5865, 2023.

[21] Yimiao Huang, Zehui Huo, Guowei Ma, Lei Zhang, Fang Wang, and Junfei Zhang. Multi-objective optimization of fly ash-slag based geopolymer considering strength, cost and CO2 emission: a new framework based on tree-based ensemble models and NSGA-II. *Journal of Building Engineering*, 68:106070, 2023.

[22] Dilshad Kakasor Ismael Jaf, Payam Ismael Abdulrahman, Ahmed Salih Mohammed, Rawaz Kurda, Shaker M.A. Qaidi, and Panagiotis G. Asteris. Machine learning techniques and multi-scale models to evaluate the impact of silicon dioxide (SiO2) and calcium oxide (CaO) in fly ash on the compressive strength of green concrete. *Construction and Building Materials*, 400:132604, 2023.

[23] Chiara F Ferraris and François DeLarrard. Testing and modeling of fresh concrete rheology. 1998.

[24] The-Duong Nguyen, Thu-Hien Tran, and Nhat-Duc Hoang. Prediction of interface yield stress and plastic viscosity of fresh concrete using a hybrid machine learning approach. *Advanced Engineering Informatics*, 44:101057, 2020.

[25] Sohaib Nazar, Jian Yang, Ayaz Ahmad, and Syed Farasat Ali Shah. Comparative study of evolutionary artificial intelligence approaches to predict the rheological properties of fresh concrete. *Materials Today Communications*, 32:103964, 2022.

[26] Ahmed Mohammed, Serwan Rafiq, Wael Mahmood, Hind Al-Darkazalir, Riyadh Noaman, Warzer Qadir, and Kawan Ghafor. Artificial Neural Network and NLR techniques to predict the rheological properties and compression strength of cement past modified with nanoclay. *Ain Shams Engineering Journal*, 12(2):1313–1328, 2021.

[27] Sohaib Nazar, Jian Yang, Muhammad Faisal Javed, Kaffayatullah Khan, Lihui Li, and Qing feng Liu. An evolutionary machine learning-based model to estimate the rheological parameters of fresh concrete. *Structures*, 48:1670–1683, 2023.

[28] Sohaib Nazar, Jian Yang, Xing-Er Wang, Kaffayatullah Khan, Muhammad Nasir Amin, Mohammad Faisal Javed, Fadi Althoey, and Mujahid Ali. Estimation of strength, rheological parameters, and impact of raw constituents of alkali-activated mortar using machine learning and SHapely Additive exPlanations (SHAP). *Construction and Building Materials*, 377:131014, 2023.

[29] Hatice Gizem Şahin, Öznur Biricik Altun, Murat Eser, Ali Mardani, and Metin Bilgin. Research on modeling the thixotropic properties of cementitious systems using regression methods in machine learning. *Construction and Building Materials*, 411:134633, 2024.

[30] Tianqi Chen and Carlos Guestrin. XGBoost: A Scalable Tree Boosting System. In *Proceedings of the 22nd ACM SIGKDD International Conference on Knowledge Discovery and Data Mining*, KDD '16, page 785–794, New York, NY, USA, 2016. Association for Computing Machinery.

[31] Scott M Lundberg and Su-In Lee. A unified approach to interpreting model predictions. In I. Guyon, U. Von Luxburg, S. Bengio, H. Wallach, R. Fergus, S. Vishwanathan, and R. Garnett, editors, *Advances in Neural Information Processing Systems*, volume 30. Curran Associates, Inc., 2017.

[32] Delphine Marchon, Shiho Kawashima, Hela Bessaies-Bey, Sara Mantellato, and Serina Ng. Hydration and rheology control of concrete for digital fabrication: Potential admixtures and cement chemistry. *Cement and Concrete Research*, 112:96–110, 2018.

[33] AlaEddin Douba, Palash Badjatya, and Shiho Kawashima. Enhancing carbonation and strength of MgO cement through 3D printing. *Construction and Building Materials*, 328:126867, 2022.

[34] Noura Khalil, Georges Aouad, Khadija El Cheikh, and Sébastien Rémond. Use of calcium sulfoaluminate cements for setting control of 3D-printing mortars. *Construction and Building Materials*, 157:382–391, 2017.

[35] Mingxu Chen, Lei Yang, Yan Zheng, Yongbo Huang, Laibo Li, Piqi Zhao, Shoude Wang, Lingchao Lu, and Xin Cheng. Yield stress and thixotropy control of 3D-printed calcium sulfoaluminate cement composites with metakaolin related to structural build-up. *Construction and Building Materials*, 252:119090, 2020.

[36] Yu Chen, Shan He, Yu Zhang, Zhi Wan, Oğuzhan Çopuroğlu, and Erik Schlangen. 3D printing of calcined clay-limestone-based cementitious materials. *Cement and Concrete Research*, 149:106553, 2021.

[37] Biranchi Panda and Ming Jen Tan. Rheological behavior of high volume fly ash mixtures containing micro silica for digital construction application. *Materials Letters*, 237:348–351, 2019.

[38] Biranchi Panda, Cise Unluer, and Ming Jen Tan. Investigation of the rheology and strength of geopolymer mixtures for extrusion-based 3D printing. *Cement and Concrete Composites*, 94:307–314, 2018.

[39] Pawel Sikora, Sang-Yeop Chung, Maxime Liard, Didier Lootens, Tobias Dorn, Paul H Kamm, Dietmar Stephan, and Mohamed Abd Elrahman. The effects of nanosilica on the fresh and hardened properties of 3D printable mortars. *Construction and Building Materials*, 281: 122574, 2021.

[40] Guan Heng Andrew Ting, Yi Wei Daniel Tay, Ye Qian, and Ming Jen Tan. Utilization of recycled glass for 3D concrete printing: Rheological and mechanical properties. *Journal of Material Cycles and Waste Management*, 21(4):994–1003, 2019.

[41] Manu K Mohan, AV Rahul, Kim Van Tittelboom, and Geert De Schutter. Rheological and pumping behaviour of 3D printable cementitious materials with varying aggregate content. *Cement and Concrete Research*, 139:106258, 2021.

[42] AV Rahul, Manu K Mohan, Geert De Schutter, and Kim Van Tittelboom. 3d printable concrete with natural and recycled coarse aggregates: Rheological, mechanical and shrinkage behaviour. *Cement and Concrete Composites*, 125:104311, 2022.

[43] John Temitope Kolawole, Riaan Combrinck, and William Peter Boshoff. Measuring the thixotropy of conventional concrete: The influence of viscosity modifying agent, superplasticiser and water. *Construction and Building Materials*, 225:853–867, 2019.

[44] Yu Chen, Stefan Chaves Figueiredo, Çağlar Yalçinkaya, Oğuzhan Çopuroğlu, Fred Veer, and Erik Schlangen. The effect of viscosity-modifying admixture on the extrudability of limestone and calcined clay-based cementitious material for extrusion-based 3D concrete printing. *Materials*, 12(9):1374, 2019.

[45] Yu Chen, Stefan Chaves Figueiredo, Zhenming Li, Ze Chang, Koen Jansen, Oğuzhan Çopuroğlu, and Erik Schlangen. Improving printability of limestone-calcined clay-based cementitious materials by using viscosity-modifying admixture. *Cement and Concrete Research*, 132: 106040, 2020.

[46] Ye Qian and Geert De Schutter. Different effects of nsf and pce superplasticizer on adsorption, dynamic yield stress and thixotropy of cement pastes. *Materials*, 11(5):695, 2018.

[47] Mingxu Chen, Xiangyang Guo, Yan Zheng, Laibo Li, Zhen Yan, Piqi Zhao, Lingchao Lu, and Xin Cheng. Effect of tartaric acid on the printable, rheological and mechanical properties of 3D printing sulphoaluminate cement paste. *Materials*, 11(12):2417, 2018.

[48] Jacques Kruger, Seung Cho, Stephan Zeranka, Celeste Viljoen, and Gideon van Zijl. 3D concrete printer parameter optimisation for high rate digital construction avoiding plastic collapse. *Composites Part B: Engineering*, 183:107660, 2020.

[49] Chenchen Sun, Jichun Xiang, Mengxue Xu, Yan He, Zhangfa Tong, and Xuemin Cui. 3D extrusion free forming of geopolymer composites: Materials modification and processing optimization. *Journal of Cleaner Production*, 258:120986, 2020.

[50] Jianzhuang Xiao, Shuai Zou, Ying Yu, Yu Wang, Tao Ding, Ying Zhu, Jiangtao Yu, Shuaishuai Li, Zhenhua Duan, Yuching Wu, et al. 3d recycled mortar printing: System development, process design, material properties and on-site printing. *Journal of Building Engineering*, 32:101779, 2020.

[51] Viacheslav Markin, Martin Krause, Jens Otto, Christof Schröfl, and Viktor Mechtcherine. 3d-printing with foam concrete: From material design and testing to application and sustainability. *Journal of Building Engineering*, 43:102870, 2021.

[52] Shin Hau Bong, Ming Xia, Behzad Nematollahi, and Caijun Shi. Ambient temperature cured 'just-add-water'geopolymer for 3D concrete printing applications. *Cement and Concrete Composites*, 121:104060, 2021.

[53] Antonio Cicione, Jacques Kruger, Richard S Walls, and Gideon Van Zijl. An experimental study of the behavior of 3D printed concrete at elevated temperatures. *Fire Safety Journal*, 120:103075, 2021.

[54] Chao Liu, Rongfei Zhang, Huawei Liu, Chunhui He, Youqiang Wang, Yiwen Wu, Shuhua Liu, Lin Song, and Fan Zuo. Analysis of the mechanical performance and damage mechanism for 3D printed concrete based on pore structure. *Construction and Building Materials*, 314:125572, 2022.

[55] Tao Ding, Jianzhuang Xiao, Shuai Zou, and Xinji Zhou. Anisotropic behavior in bending of 3D printed concrete reinforced with fibers. *Composite Structures*, 254:112808, 2020.

[56] Yanqun Xu, Qiang Yuan, Zemin Li, Caijun Shi, Qihong Wu, and Yanlin Huang. Correlation of interlayer properties and rheological behaviors of 3DPC with various printing time intervals. *Additive Manufacturing*, 47:102327, 2021.

[57] SH Chu, LG Li, and AKH Kwan. Development of extrudable high strength fiber reinforced concrete incorporating nano calcium carbonate.

Additive Manufacturing, 37:101617, 2021.

[58] Thadshajini Suntharalingam, Brabha Nagaratnam, Keerthan Poologanathan, Phil Hackney, and Jeffri Ramli. Effect of polypropylene fibres on the mechanical properties of extrudable cementitious material. In *Second RILEM International Conference on Concrete and Digital Fabrication: Digital Concrete 2020 2*, pages 516–526. Springer, 2020.

[59] Yu Chen, Koen Jansen, Hongzhi Zhang, Claudia Romero Rodriguez, Yidong Gan, Oğuzhan Çopuroğlu, and Erik Schlangen. Effect of printing parameters on interlayer bond strength of 3D printed limestone-calcined clay-based cementitious materials: An experimental and numerical study. *Construction and Building Materials*, 262:120094, 2020.

[60] Bilal Baz, Georges Aouad, and Sebastien Remond. Effect of the printing method and mortar's workability on pull-out strength of 3D printed elements. *Construction and Building Materials*, 230:117002, 2020.

[61] Huajian Li, Fali Huang, Yongjiang Xie, Zhonglai Yi, and Zhen Wang. Effect of water–powder ratio on shear thickening response of scc. *Construction and Building Materials*, 131:585–591, 2017.

[62] Abdulrahman Albar, Mehdi Chougan, Mazen J Al-Kheetan, Mohammad Rafiq Swash, and Seyed Hamidreza Ghaffar. Effective extrusion-based 3D printing system design for cementitious-based materials. *Results in Engineering*, 6:100135, 2020.

[63] Mohammad Amin Moeini, Masoud Hosseinpoor, and Ammar Yahia. Effectiveness of the rheometric methods to evaluate the build-up of cementitious mortars used for 3D printing. *Construction and Building Materials*, 257:119551, 2020.

[64] AV Rahul and Manu Santhanam. Evaluating the printability of concretes containing lightweight coarse aggregates. *Cement and Concrete Composites*, 109:103570, 2020.

[65] Hojae Lee, Jang-Ho Jay Kim, Jae-Heum Moon, Won-Woo Kim, and Eun-A Seo. Evaluation of the mechanical properties of a 3D-printed mortar. *Materials*, 12(24):4104, 2019.

[66] M Papachristoforou, V Mitsopoulos, and M Stefanidou. Evaluation of workability parameters in 3D printing concrete. *Procedia Structural Integrity*, 10:155–162, 2018.

[67] Daniel Heras Murcia, Moneeb Genedy, and MM Reda Taha. Examining the significance of infill printing pattern on the anisotropy of 3D printed concrete. *Construction and Building Materials*, 262:120559, 2020.

[68] Weiqiang Wang, Nikolaos Konstantinidis, Simon A Austin, Richard A Buswell, Sergio Cavalaro, and Domenico Cecinia. Flexural behaviour of AR-glass textile reinforced 3D printed concrete beams. In *Second RILEM International Conference on Concrete and Digital Fabrication: Digital Concrete 2020 2*, pages 728–737. Springer, 2020.

[69] Yeşim Tarhan and Remzi Şahin. Fresh and rheological performances of air-entrained 3D printable mortars. *Materials*, 14(9):2409, 2021.

[70] Yu Zhang, Yunsheng Zhang, Lin Yang, Guojian Liu, Yidong Chen, Shiwei Yu, and Hongjian Du. Hardened properties and durability of large-scale 3D printed cement-based materials. *Materials and Structures*, 54:1–14, 2021.

[71] Mehdi Chougan, Seyed Hamidreza Ghaffar, Pawel Sikora, Sang-Yeop Chung, Teresa Rucinska, Dietmar Stephan, Abdulrahman Albar, and Mohammad Rafiq Swash. Investigation of additive incorporation on rheological, microstructural and mechanical properties of 3D printable alkali-activated materials. *Materials & Design*, 202:109574, 2021.

[72] Sooraj AO Nair, Hussam Alghamdi, Aashay Arora, Iman Mehdipour, Gaurav Sant, and Narayanan Neithalath. Linking fresh paste microstructure, rheology and extrusion characteristics of cementitious binders for 3D printing. *Journal of the American Ceramic Society*, 102 (7):3951–3964, 2019.

[73] AV Rahul, Manu Santhanam, Hitesh Meena, and Zimam Ghani. Mechanical characterization of 3D printable concrete. *Construction and Building Materials*, 227:116710, 2019.

[74] Mingxu Chen, Lei Yang, Yan Zheng, Laibo Li, Shoude Wang, Yongbo Huang, Piqi Zhao, Lingchao Lu, and Xin Cheng. Rheological behaviors and structure build-up of 3D printed polypropylene and polyvinyl alcohol fiber-reinforced calcium sulphoaluminate cement composites. *Journal of Materials Research and Technology*, 10:1402–1414, 2021.

[75] Mingxu Chen, Laibo Li, Jiaao Wang, Yongbo Huang, Shoude Wang, Piqi Zhao, Lingchao Lu, and Xin Cheng. Rheological parameters and building time of 3D printing sulphoaluminate cement paste modified by retarder and diatomite. *Construction and Building Materials*, 234: 117391, 2020.

[76] Mingxu Chen, Bo Liu, Laibo Li, Lidong Cao, Yongbo Huang, Shoude Wang, Piqi Zhao, Lingchao Lu, and Xin Cheng. Rheological parameters, thixotropy and creep of 3D-printed calcium sulfoaluminate cement composites modified by bentonite. *Composites Part B: Engineering*, 186:107821, 2020.

[77] Bing Lu, Weiping Zhu, Yiwei Weng, Zhixin Liu, En-Hua Yang, Kah Fai Leong, Ming Jen Tan, Teck Neng Wong, and Shunzhi Qian. Study of MgO-activated slag as a cementless material for sustainable spray-based 3D printing. *Journal of Cleaner Production*, 258:120671, 2020.

[78] Jolien Van Der Putten, Geert De Schutter, and Kim Van Tittelboom. Surface modification as a technique to improve inter-layer bonding strength in 3D printed cementitious materials. *RILEM Technical Letters*, 4:33–38, 2019.

[79] Mehdi Chougan, Seyed Hamidreza Ghaffar, Mohammad Jahanzat, Abdulrahman Albar, Nahzatullah Mujaddedi, and Rafiq Swash. The influence of nano-additives in strengthening mechanical performance of 3D printed multi-binder geopolymer composites. *Construction and Building Materials*, 250:118928, 2020.

[80] Fali Huang, Huajian Li, Zhonglai Yi, Zhen Wang, and Yongjiang Xie. The rheological properties of self-compacting concrete containing superplasticizer and air-entraining agent. *Construction and Building Materials*, 166:833–838, 2018.

[81] Da-Wang Zhang, Dong min Wang, Xi-Qiang Lin, and Tao Zhang. The study of the structure rebuilding and yield stress of 3D printing geopolymer pastes. *Construction and Building Materials*, 184:575–580, 2018.

[82] Brahim Mazhoud, Arnaud Perrot, Vincent Picandet, Damien Rangeard, and Eric Courteille. Underwater 3D printing of cement-based mortar. *Construction and Building Materials*, 214:458–467, 2019.

[83] Atta Ur Rehman, Sang-Min Lee, and Jung-Hoon Kim. Use of municipal solid waste incineration ash in 3D printable concrete. *Process Safety and Environmental Protection*, 142:219–228, 2020.

[84] Jie Xu, Lieyun Ding, Lixiong Cai, Lichao Zhang, Hanbin Luo, and Wenbo Qin. Volume-forming 3D concrete printing using a variable-size square nozzle. *Automation in Construction*, 104:95–106, 2019.

[85] Yu Chen, Claudia Romero Rodriguez, Zhenming Li, Boyu Chen, Oğuzhan Çopuroğlu, and Erik Schlangen. Effect of different grade levels of calcined clays on fresh and hardened properties of ternary-blended cementitious materials for 3D printing. *Cement and Concrete Composites*, 114:103708, 2020.
[86] Suvash Chandra Paul, Yi Wei Daniel Tay, Biranchi Panda, and Ming Jen Tan. Fresh and hardened properties of 3D printable cementitious materials for building and construction. *Archives of Civil and Mechanical Engineering*, 18(1):311–319, 2018.
[87] A.V. Rahul, Manu Santhanam, Hitesh Meena, and Zimam Ghani. 3D printable concrete: Mixture design and test methods. *Cement and Concrete Composites*, 97:13–23, 2019.
[88] Qiang Yuan, Zemin Li, Dajun Zhou, Tingjie Huang, Hai Huang, Dengwu Jiao, and Caijun Shi. A feasible method for measuring the buildability of fresh 3D printing mortar. *Construction and Building Materials*, 227:116600, 2019.
[89] Guowei Ma, Nazar Muhammad Salman, Li Wang, and Fang Wang. A novel additive mortar leveraging internal curing for enhancing interlayer bonding of cementitious composite for 3D printing. *Construction and Building Materials*, 244:118305, 2020.
[90] Daniel G. Soltan and Victor C. Li. A self-reinforced cementitious composite for building-scale 3D printing. *Cement and Concrete Composites*, 90:1–13, 2018.
[91] Jacques Kruger, Stephan Zeranka, and Gideon van Zijl. An ab initio approach for thixotropy characterisation of (nanoparticle-infused) 3D printable concrete. *Construction and Building Materials*, 224:372–386, 2019.
[92] Stefan Chaves Figueiredo, Claudia Romero Rodríguez, Zeeshan Y Ahmed, Derk H Bos, Yading Xu, Theo M Salet, Oğuzhan Çopuroğlu, Erik Schlangen, and Freek P Bos. An approach to develop printable strain hardening cementitious composites. *Materials & Design*, 169: 107651, 2019.
[93] Biranchi Panda, Suvash Chandra Paul, and Ming Jen Tan. Anisotropic mechanical performance of 3D printed fiber reinforced sustainable construction material. *Materials Letters*, 209:146–149, 2017.
[94] Ali Kazemian, Xiao Yuan, Evan Cochran, and Behrokh Khoshnevis. Cementitious materials for construction-scale 3D printing: Laboratory testing of fresh printing mixture. *Construction and Building Materials*, 145:639–647, 2017.
[95] Binrong Zhu, Jinlong Pan, Behzad Nematollahi, Zhenxin Zhou, Yang Zhang, and Jay Sanjayan. Development of 3D printable engineered cementitious composites with ultra-high tensile ductility for digital construction. *Materials & Design*, 181:108088, 2019.
[96] Yi Wei Daniel Tay, Ming Yang Li, and Ming Jen Tan. Effect of printing parameters in 3D concrete printing: Printing region and support structures. *Journal of Materials Processing Technology*, 271:261–270, 2019.
[97] Venkatesh Naidu Nerella, Simone Hempel, and Viktor Mechtcherine. Effects of layer-interface properties on mechanical performance of concrete elements produced by extrusion-based 3D-printing. *Construction and Building Materials*, 205:586–601, 2019.
[98] Yidong Chen, Yunsheng Zhang, Bo Pang, Zhiyong Liu, and Guojian Liu. Extrusion-based 3D printing concrete with coarse aggregate: Printability and direction-dependent mechanical performance. *Construction and Building Materials*, 296:123624, 2021.
[99] Yu Zhang, Yunsheng Zhang, Guojian Liu, Yonggan Yang, Meng Wu, and Bo Pang. Fresh properties of a novel 3D printing concrete ink. *Construction and Building Materials*, 174:263–271, 2018.
[100] Tao Ding, Jianzhuang Xiao, Shuai Zou, and Yu Wang. Hardened properties of layered 3D printed concrete with recycled sand. *Cement and Concrete Composites*, 113:103724, 2020.
[101] Biranchi Panda, Shaoqin Ruan, Cise Unluer, and Ming Jen Tan. Improving the 3D printability of high volume fly ash mixtures via the use of nano attapulgite clay. *Composites Part B: Engineering*, 165:75–83, 2019.
[102] VN Nerella, M Näther, A Iqbal, M Butler, and V Mechtcherine. Inline quantification of extrudability of cementitious materials for digital construction. *Cement and Concrete Composites*, 95:260–270, 2019.
[103] Babak Zareiyan and Behrokh Khoshnevis. Interlayer adhesion and strength of structures in Contour Crafting-Effects of aggregate size, extrusion rate, and layer thickness. *Automation in Construction*, 81:112–121, 2017.
[104] Viktor Mechtcherine, Venkatesh Naidu Nerella, Frank Will, Mathias Näther, Jens Otto, and Martin Krause. Large-scale digital concrete construction–CONPrint3D concept for on-site, monolithic 3D-printing. *Automation in Construction*, 107:102933, 2019.
[105] Biranchi Panda, Suvash Chandra Paul, Nisar Ahamed Noor Mohamed, Yi Wei Daniel Tay, and Ming Jen Tan. Measurement of tensile bond strength of 3D printed geopolymer mortar. *Measurement*, 113:108–116, 2018.
[106] Guowei Ma, Zhijian Li, Li Wang, Fang Wang, and Jay Sanjayan. Mechanical anisotropy of aligned fiber reinforced composite for extrusion-based 3D printing. *Construction and Building Materials*, 202:770–783, 2019.
[107] Thanh T Le, Simon A Austin, Sungwoo Lim, Richard A Buswell, Alistair GF Gibb, and Tony Thorpe. Mix design and fresh properties for high-performance printing concrete. *Materials and Structures*, 45:1221–1232, 2012.
[108] Guowei Ma, Zhijian Li, and Li Wang. Printable properties of cementitious material containing copper tailings for extrusion based 3D printing. *Construction and Building Materials*, 162:613–627, 2018.
[109] Luong Pham, Phuong Tran, and Jay Sanjayan. Steel fibres reinforced 3D printed concrete: Influence of fibre sizes on mechanical performance. *Construction and Building Materials*, 250:118785, 2020.
[110] Arnaud Perrot, Damien Rangeard, and Alexandre Pierre. Structural built-up of cement-based materials used for 3D-printing extrusion techniques. *Materials and Structures*, 49:1213–1220, 2016.
[111] Biranchi Panda, Nisar Ahamed Noor Mohamed, Suvash Chandra Paul, GVP Bhagath Singh, Ming Jen Tan, and Branko Šavija. The effect of material fresh properties and process parameters on buildability and interlayer adhesion of 3D printed concrete. *Materials*, 12(13):2149, 2019.
[112] Taylor Marchment, Jay Sanjayan, and Ming Xia. Method of enhancing interlayer bond strength in construction scale 3D printing with mortar by effective bond area amplification. *Materials & Design*, 169:107684, 2019.
[113] Jianhao Gao, Zijie Wang, and Chaofeng Wang. 3D printing concrete mix design open dataset, June 2023. URL https://doi.org/10.5281/zenodo.8070144.
[114] S.H. Chu. Volume-based design of ultra-low cement concrete. *Construction and Building Materials*, 391:131405, 2023.
[115] Nick Erickson, Jonas Mueller, Alexander Shirkov, Hang Zhang, Pedro Larroy, Mu Li, and Alexander Smola. AutoGluon-Tabular: Robust

and accurate AutoML for structured data. *arXiv preprint arXiv:2003.06505*, 2020.